Chapter 2
Silicon-Based Frequency References

This chapter provides an overview of silicon-based frequency references. Reduction of size and cost as well as increased reliability have been the main motivations for the realization of on-chip frequency references. However, the main limitation of such references is the effect of variations in process, voltage, and temperature (PVT) on their output frequency. This chapter reviews various state-of-the-art implementations of silicon-based frequency references. These have been mainly introduced in the open literature or available as products on the market. The chapter's main goal is to provide an overview of the pros and cons of the selected approaches in order to build a comparison chart. Such overview should help the reader to make a comparison between the approach described in this book, electrothermal frequency references, and the other available solutions.

2.1 Introduction

The stability of a frequency reference is a measure of the amount of variation in its output frequency as a function of environmental parameters. These include temperature, supply voltage, process tolerances, noise, etc. It should be noted that the terms stability and accuracy will be used interchangeably throughout this book. This is because they both refer to the same concept as far as the level of variations in the nominal oscillation frequency of an oscillator is concerned. If this nominal value is equal to f_0, then its level of stability (accuracy) is measured either in parts per million (ppm) or in percent [1–4]. If the absolute value of the deviation in the output frequency is Δf, then the error can be calculated as:

$$f_{error}(\%) = \frac{\Delta f}{f_0} \cdot 10^2 \quad \text{or} \quad f_{error}(ppm) = \frac{\Delta f}{f_0} \cdot 10^6. \tag{2.1}$$

S.M. Kashmiri and K.A.A. Makinwa, *Electrothermal Frequency References in Standard CMOS*, Analog Circuits and Signal Processing,
DOI 10.1007/978-1-4614-6473-0_2, © Springer Science+Business Media New York 2013

Various electronic systems require different levels of accuracy for their frequency references. For instance, in some microcontroller applications references stable from 0.01% (100 ppm) to 1% (10,000 ppm) [5] might be required, while a wire-line data link such as USB 2.0 needs 500 ppm of clock accuracy [6]. Wireless communication channels require tighter accuracies. For instance a cell-phone handset application might need frequencies stable to 2.5 ppm [7], while a GPS receiver or a mobile base-station system might require sub-ppm accuracies [3, 7].

For decades, crystal oscillators have been the only means of producing stable frequencies. Considering their low temperature dependency, relatively low cost and small form factor, as well as their wide commercial availability, they have a dominant share of the frequency control market (more than 90%, equivalent to more than 4.5 billion dollars) [3]. Quartz crystal oscillators are available with various levels of accuracy. The non-compensated (XO) and voltage compensated (VCXO) oscillators achieve stabilities in the range of 20–100 ppm. When they are temperature compensated (TCXO), their accuracy is in the 0.1–5 ppm range. Oven controlled (OCXO) oscillators achieve very high stabilities: in the order of 1 ppb (part per billion) [3].

Apart from their high levels of accuracy, quartz crystal oscillators also have some drawbacks. The first of them is the space they occupy on printed circuit boards, especially when a number of frequency sources are required within one system. Another important disadvantage is their sensitivity to mechanical shock and vibration. This mainly affects the quartz crystal, which is in fact an electro-mechanical part [3]. Compared to electronic circuits, whose functionality is due to the movement of electrons, the crystal vibrates at the frequency of oscillation. This means that any physical motion of the crystal will change its frequency [3].

The abovementioned limitations have driven the search for integrated frequency references that can achieve the same level of stability as quartz crystal oscillators. Such references will be manufactured in silicon, which is why they are also referred to as silicon-based frequency references [8].

As early as 1967, the first steps towards frequency generation by means of MEMS (micro-machined silicon) structures were taken [9]. Around 1968, the concept of a self-referenced silicon frequency reference was illustrated with a temperature-compensated Wien-bridge RC oscillator. Later, various types of electrical oscillators such as RC, relaxation, ring, and LC oscillators have been proposed. Among these methods, MEMS-based and LC-based oscillators have been commercialized and currently achieve performance levels that can compete with crystal oscillators. In this chapter, an overview of these methods of silicon-based frequency generation will be described. State-of-the-art references will be studied in regard to their system-level architecture, their achieved level of accuracy, as well as an overview of their potential applications.

Since this book is about CMOS compatible frequency references, crystal oscillators will not be further discussed. Furthermore, MEMS-based oscillators, which are not truly standard CMOS compatible, will be briefly introduced in the next section. The chapter progresses with a more detailed overview of

CMOS-based LC, RC, relaxation, and ring oscillators. Furthermore, a new class of ultra-low-power frequency references based on the electron mobility of MOS transistors will be introduced. Finally, a comparison between these methods will be provided.

2.2 Silicon MEMS Based Oscillators

Quartz crystal resonators are excited at their resonance frequency by an electrical oscillator circuit. Their operation depends on the piezoelectric properties of a material that cannot be integrated in IC technology: quartz. Over the years, a lot of research has been done on the development of silicon MEMS (Micro Electro Mechanical Systems) based resonators with the aim of replacing quartz crystals. MEMS technology involves many of the processes used by the integrated circuit technology such as lithography, deposition, etching, etc. [10]. This technology has been applied in sensors such as accelerometers, gyroscopes, microphones, etc.

MEMS resonators are micro-machined structures that can vibrate at their resonance frequency if an external excitation is applied to them. The resonance property of such structures was first researched in 1967, when a resonant gate transistor was presented as a micro-machined integrated frequency reference [11]. This excitation can be of the electrostatic, piezoelectric or electromagnetic type [12, 13]. The *Quality* factor of a resonator determines the stability of the frequency reference that is built around it. It is the ratio of its peak resonance frequency to the width of the peak. A MEMS resonator's shape and geometry determines this factor, which is typically between 50,000 and 300,000, a range that is comparable to quartz crystal oscillators [12, 13].

MEMS resonators have faced many challenges in delivering a cost-effective and reliable solution that could compete commercially with quartz crystals. The major challenges included packaging, vibration and shock sensitivity, temperature drift and long term stability [14]. In recent years various commercial products have been introduced by two start-up companies: Discera and SiTime. Discera was established in 2001 based on research on MEMS resonators funded by DARPA, while SiTime started in 2004 based on IP licensed through Bosch [3]. Today, MEMS-based frequency references produced by these companies are more compact than their quartz competitors and are more cost effective due to the mass production allowed by the use of IC technology. However, their level of jitter (phase noise) is not (yet) low enough for cell-phone applications.

Because of the special processing required by MEMS technology, a MEMS resonator has to be manufactured on a separate die from the die that holds the electronic circuitry exciting and controlling it [12–14]. Furthermore, the mass of a MEMS resonator is small, being on the order of 10^{-14}–10^{-11} kg, which means that its resonance frequency and quality factor will be affected by any gas molecules surrounding it [15]. This means that silicon MEMS resonators should preferably be

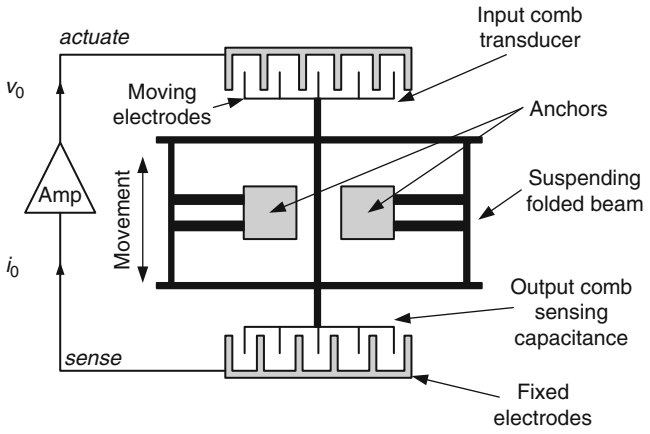

Fig. 2.1 Simplified block-diagram of a silicon MEMS based oscillator

operated in vacuum, which is the reason why they have been fabricated within silicon cavities [12–14].

Another challenge in making MEMS-based oscillators is the temperature dependence of MEMS resonators. This is due to the temperature coefficient of the Young's modulus of silicon [3, 12, 13]. This is in the order of 20–40 ppm/°C, which is larger than that of quartz and necessitates a means for the temperature compensation of such oscillators. There have been various structural techniques proposed to reduce or correct for the MEMS resonator's temperature coefficient. These include the combination of materials with positive and negative thermal stiffness coefficients or the application of an electric field to control the resonator's stiffness [16]. The approach that has been ultimately used in commercial products is to correct the temperature dependence of the oscillator through a fractional frequency synthesizer and a temperature sensor [17]. This technique will be described later.

An encapsulated silicon MEMS resonator needs to be attached to an anchor on a substrate [14]. Figure 2.1, shows a conceptual and simplified drawing of a MEMS resonator [18]. Folded suspending beams are anchored to the silicon substrate at two anchor points. The suspending beams are connected to the sides of comb transducer structures. The resonator structure is biased with a DC bias source. The output transducer experiences a change in capacitance due to the movement of the suspending beam with reference to the fixed electrodes. This causes an electrical signal, i_o, which is fed to an electronic circuit that produces an excitation signal v_o, which is then applied to the input transducer. This signal will electrostatically actuate the resonator. The structure vibrates at its resonance frequency (typically in the hundreds of kHz to MHz range), which is the same frequency at which it is excited electrically. The required electrical signal is in fact the output signal of the oscillator.

The MEMS frequency references produced by SiTime consist of a resonator element, which is wire bonded to a CMOS die that includes a sustaining circuitry,

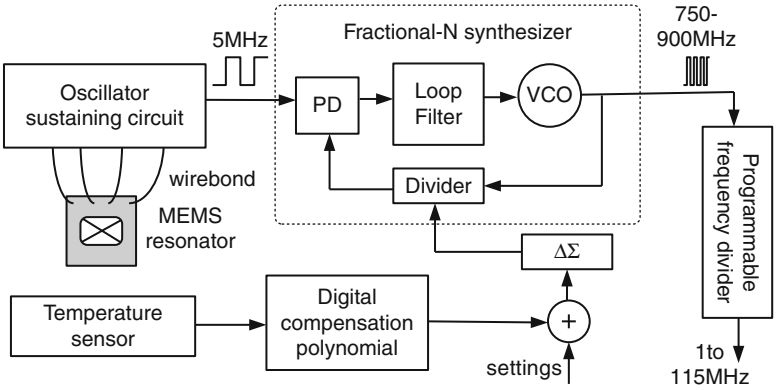

Fig. 2.2 Simplified block-diagram of a silicon MEMS oscillator, including a MEMS resonator, a fractional-N synthesizer and a temperature compensation scheme

a high-resolution fractional-N frequency synthesizer [19], a temperature sensor and digital circuitry [12–14, 17]. A simplified block diagram of this system [17] is shown in Fig. 2.2. The MEMS resonator vibrates at 5 MHz, which is the same frequency as that of the sustaining circuitry. This 5 MHz signal is provided to the fractional-N synthesizer, which outputs a higher frequency: in the range of 750–900 MHz [17]. This frequency can be adjusted with sub-ppm resolution over a 10% tuning range. A programmable output frequency can then be produced by dividing the output of the synthesizer. The advantage of this approach is that the same MEMS resonator can be used to provide different output frequencies. This means that the output frequency can be easily programmed into the device depending on the application.

The temperature dependence of the MEMS resonator is compensated by measuring the temperature of the CMOS die with an embedded temperature sensor. The temperature information is digitally processed through a compensation polynomial whose coefficients are stored in a non-volatile memory. The frequency reference achieves a part to part frequency stability of about 10 ppm from −40°C to 85°C [17]. In this approach, the jitter performance of the output frequency is determined by the frequency synthesizer (that is in principle a PLL). For better jitter performance, low noise and high quality factor oscillators such as LC based resonance circuits have been combined with optimized PLLs as well as power supply regulation techniques [13, 17].

One of the concerns regarding MEMS oscillators has been about their reliability in comparison to the mature quartz crystal rival. Since a MEMS resonator is a mechanical device that vibrates at millions of cycles per second, aging is one of these reliability concerns. Reliability tests published by Discera, show sub-ppm shifts in the first year of operation of such devices [20]. Furthermore, due to their very small dimensions (micro-meter range) and very small weight, MEMS resonators have better shock resistance than quartz crystals [20]. Further reliability tests such as vibration resistance, sensitivity to packaging vacuum, thermal cycling

and high temperature storage life have been reported in [20], showing that MEMS frequency references can compete with crystal oscillators.

Most commercial MEMS frequency references are manufactured by SiTime [21] and Discera [22]. SiTime's high performance oscillators include the SiT8208, SiT8102 and SiT9102 in standard six-pin packages (5.0×3.2 mm^2), which are smaller than those currently used for quartz crystals [13]. SiTime also introduced very thin SiT8003 oscillators with 0.25 mm thick packages, mainly intended for SIM card, camera, and cell phone applications. SiTime's range of products cover output frequency stabilities from sub-ppm to 50 ppm over the commercial and industrial temperature range (-40°C to 85°C). The high performance SiT8208 and SiT8209 products have sub-ps output jitter [23].

Discera's MEMS frequency references use the same technique of combining a MEMS resonator with a PLL [22]. Their range of stability is about 50 ppm, at supply voltages of 1.8–3.3 V, output frequencies of 1–150 MHz and supply currents in the order of 3 mA. They are available in standard packages that can be placed in crystal oscillator footprints. Their intended applications are in: mobile applications, consumer electronics, portable electronics, CCD clocks for cameras, etc.

So far, the commercially introduced MEMS frequency references show that sub-ppm frequency stabilities and programmable output frequencies are feasible. Furthermore, their small footprints make it possible to replace standard crystals with MEMS-based devices. However, they still have a few drawbacks. Their jitter performance is determined by their fractional-N synthesizer and by the temperature compensation scheme. Also, the special processing required for the MEMS resonator makes single die integration of these devices difficult. This means that the integration of such frequency references as an IP block in a system-on-chip will usually result in a two-chip solution.

2.3 LC Oscillators

Another class of commercially available frequency references are the LC oscillators [24]. Such oscillators operate at the resonance frequency of an LC tank [25] and have been widely used in VCO's that produce RF range of frequencies [26]. These VCO's have been normally embedded into phase-locked loops (PLLs), with the aim of frequency synthesis from an external reference source. In order to function as a self-referenced frequency source, an LC oscillator needs to be free-running. In this case, special attention needs to be paid to its output frequency stability as a function of process, temperature and voltage variations. An LC oscillator is based on passive elements such as inductors and capacitors as well as active elements, i.e. transistors. Therefore, such an oscillator can be made in a standard CMOS process.

The first steps towards commercializing self-referenced LC oscillators were taken at Mobius Microsystems, a fab-less company founded in 2004 with the aim of developing all-silicon frequency sources that replace quartz crystal oscillators. The goal of Mobius Microsystems was to produce a monolithic free running RF LC

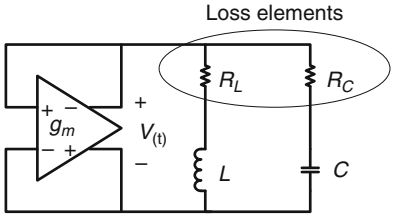

Fig. 2.3 Simplified block diagram of an LC oscillator including the LC elements as well as their equivalent losses

oscillator that did not require the frequency synthesizers used in MEMS frequency references. This was to avoid the effect of multiplication on the output frequency jitter. These efforts resulted in oscillators with output frequency ranges from 12 to 25 MHz and with initial target applications such as wire-line data communication, e.g. USB [27–32]. These solutions achieved output frequency stabilities in the order of 100 ppm with period jitters in the order of 3–6 ps (rms). In 2010, Mobius Microsystems was acquired by IDT, who has subsequently introduced LC oscillator based frequency references to the market [24].

A simplified block diagram of an LC oscillator is shown in Fig. 2.3. It includes an LC tank with inductor and capacitor values of L and C, respectively, each with their equivalent finite losses, R_L and R_C [31]. It also has a sustaining transconductor amplifier g_m (cross-coupled pairs) that compensates for the loss in the tank. The oscillation frequency is then [31]:

$$\omega = \frac{1}{LC}\sqrt{\frac{L - C \cdot R_L^2}{L - C \cdot R_C^2}}. \tag{2.2}$$

An LC oscillator based on the resonant tank shown in Fig. 2.3, not only suffers from frequency deviation due to the losses, but also due to variations in the absolute values of the passive elements due to process and temperature. The absolute values of integrated inductances have negligible temperature coefficient [31, 33], however, the temperature dependence of their equivalent loss resistance, R_L, is determined by the material from which the inductor is made. Since R_L is usually larger than R_C, the former's temperature dependence will be dominant. Furthermore, the capacitance will be affected by the fringing capacitors due to interconnect and parasitic capacitances of the transconductor g_m. The latter capacitance then has considerable temperature and bias dependence [31]. In principle, the temperature dependence of the output frequency of an LC oscillator shows a concave negative temperature coefficient, whose sensitivity increases at high temperatures [31].

The output frequency of an LC oscillator can also be affected if conducting materials are in its vicinity, since the field lines of the inductor will be affected by changes in the permeability or due to eddy currents [31, 32]. To overcome this problem, the solution proposed by IDT [32] is to build a Faraday shield around the die in order to maintain the fringing field lines and avoid disturbances. This is done by depositing a thick dielectric layer on the die of the LC oscillator chip, and

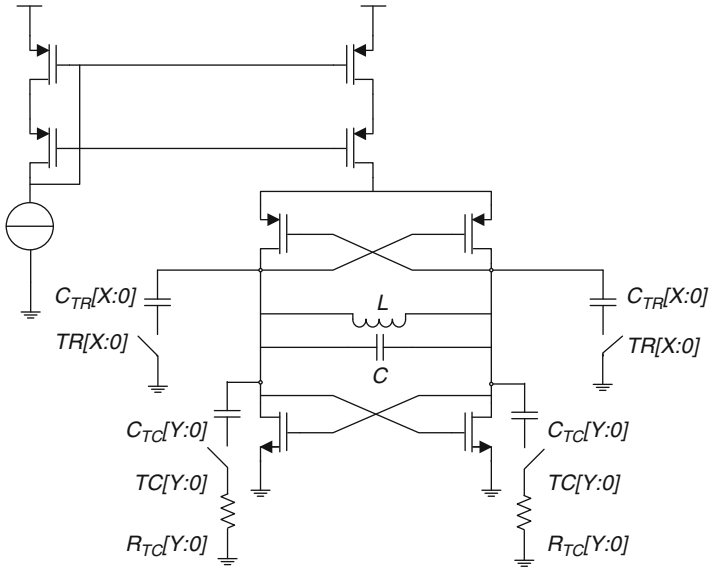

Fig. 2.4 Simplified circuit diagram of an LC oscillator and the trimming and temperature compensation networks

electroplating several microns of Cupper on top of that. The back side of the device is also shielded by means of an Aluminum layer [32].

A simplified circuit block diagram of the LC based oscillator used in the core of the frequency reference initially proposed by Mobius Microsystems and later turned into a product by IDT is shown in Fig. 2.4 [32]. In the initial publication [28] the resonance frequency was 1 GHz, which was later increased to 3 GHz [32] to increase the quality factor of the inductor. The LC oscillator consists of a cross-coupled negative transconductance amplifier with PMOS biasing transistors for low $1/f$ noise operation. An array of thin film programmable capacitors C_{TR}[X:0] connected through the corresponding switches TR[X:0] are used to trim the output frequency. A set of thin film capacitors C_{TC}[Y:0] and series resistors R_{TC}[Y:0] can be connected through switches TC[Y:0], which are used to introduce a loss to the capacitive network. The type of RC network is chosen such that its temperature dependence works against that of the inductor's loss resistance to minimize the nonlinearity in the temperature coefficient of the oscillator [32]. The frequency reference includes a low drop-out regulator (LDO) to reduce the effect of power supply fluctuations, as well as a programmable divider allowing for programmable output frequency.

The LC oscillator introduced in [25] (0.35 µm CMOS) had an output frequency of 12 MHz and a supply current of 9.5 mA. It achieved a stability of about 400 ppm from $-10°$C to 85°C and a period jitter of <10 ps (rms). The work in [28] (0.25 µm CMOS) achieved a frequency stability of 90 ppm (shown for one device) from 0°C to 70°C. This work used an active temperature compensation scheme and dissipated

about 15 mA. Its output jitter was <7 ps (rms). A major modification to these devices, towards reduction of their power consumption, was the change in their temperature compensation schemes. This initially included an active temperature compensation block including a PTAT generator and varactors in the LC tank, which were attached to a temperature dependent control voltage [29–31]. Later, this was changed to the passive temperature compensation scheme described in Fig. 2.4 [32]. As a result the supply current was reduced from 15 mA in [28] to less than 2 mA in [24, 32]. The frequency stability of these oscillators was about 300 ppm from 0°C to 70°C with a period jitter of 3.5 ps (rms). The recent product published by IDT [34] combines the previous active and passive temperature compensation schemes, adds an improved Faraday shield to solve the problem of interfering fields with the oscillator's resonance, and a two-point temperature trim to achieve a stability of <50 ppm from −20°C to 70°C and a sub-ps jitter level. Apart from the products introduced by IDT, the Si500 LC oscillators have been introduced by Silicon Labs [35]. These are capable of producing frequencies programmable from 0.9 to 200 MHz and are realized in a 0.13 μm CMOS. They draw 8 mA from a 1.8 V supply and are operational from 0°C to 70°C with stabilities in the order of 150 ppm.

Considering the number of temperature and process dependent variables in LC oscillators and the probable lack of correlation between these parameters, a single-point temperature trim is not sufficient for these devices. However, multiple point trims add to the production costs. Furthermore, LC oscillators have rather narrow temperature ranges, in the order of −20°C to 70°C, limiting their application operating over wide temperature ranges.

2.4 RC Harmonic Oscillators

The next class of oscillator reviewed here is the RC harmonic oscillator. This type of oscillator uses resistors and capacitors to form an RC network, which functions as a frequency selection circuit, and which can be combined with an amplifier to realize a linear oscillator with a sinusoidal output signal [36]. The output frequency of RC oscillators will be affected by variations in the absolute value of on-chip resistors and capacitors as well as their temperature dependence [37–39]. These variations can be in the order of tens of percent. By means of trimming and temperature compensation the stability of RC oscillators reaches about 1% [40]. Despite their lower accuracy, compared to the LC oscillators, RC oscillators are suitable for low frequency (hundreds of kHz to a few MHz) as well as low power (tens of micro-Watts) applications [40–43].

A well known type of harmonic RC oscillator is the Wien-bridge oscillator. This is based on an electrical network proposed by Max Wien in 1891 [40, 44]. As shown in Fig. 2.5, it includes two resistors and capacitors. The complete oscillator can be seen as a positive feedback amplifier with a band-pass network in its feedback path. In 1939, William Hewlett, a co-founder of Hewlett-Packard Company (HP),

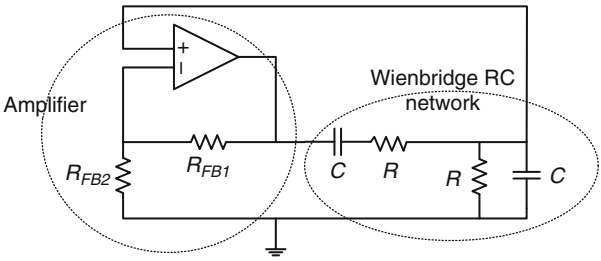

Fig. 2.5 Simplified circuit diagram of a Wien-bridge harmonic RC oscillator

designed a Wien-bridge oscillator while an MSc student at Stanford University. This later led to HP200A, one of the first products of HP [45, 46], which was a low distortion oscillator for audio applications.

A remarkable point regarding the HP200A was its use of an incandescent bulb as a positive temperature coefficient thermistor in the oscillator's feedback path (R_{FB2}). This was for amplitude regulation. Without this, the output signal of the oscillator increases until it clips at the supply rails, thus creating harmonic distortion. The use of the bulb in the feedback path means that amplitude growth causes current increase, which heats the bulb, increasing its resistance and causing the current to decrease.

The Wien-bridge harmonic RC oscillator shown in Fig. 2.5 oscillates when the amplifier has a gain of 3 [40]. This gain is set by means of the resistive feedback network around the amplifier. At a gain of 3, the circuit will oscillate at:

$$f_{osc} = \frac{1}{2\pi RC}. \tag{2.3}$$

with R and C being the values of the elements in the passive feedback network. The network has a quality factor $Q = 1/3$ [40]. To first order, the process and temperature stability of this frequency are determined only by that of the passive R and C elements. In the implementation reported in [40], metal-insulator-metal (MiM) types of capacitors have been used, whose temperature dependence is reported to be negligible. In addition, positive temperature coefficient N-poly resistors were combined with negative temperature coefficient P-poly resistors, leading to a residual temperature coefficient of 36 ppm/°C. The remaining source of spread is the variation in the absolute values of these elements, which can be up to 10%, requiring a process trim to be applied to the oscillator.

Other non-idealities contributing to the inaccuracy of the output frequency are related to the finite gain, output impedance and the phase shift introduced by the amplifier. In order to mitigate their effects, the fully differential and modified Wien-bridge oscillator circuit shown in Fig. 2.6 has been proposed [40, 41]. Transistor T_1 forms the amplifier, which is degenerated by R_{deg} and cascoded by gain-boosted cascode transistors T_2 and T_3 (gain-boosters not shown), and biased with extra current-bleeding sources I_b. Resistor degeneration has been used to guarantee that the amplifier's gain of 3 is defined by the ratio R/R_{deg}. To enhance the degeneration by maximizing the transconductance of T_1 and without sacrificing

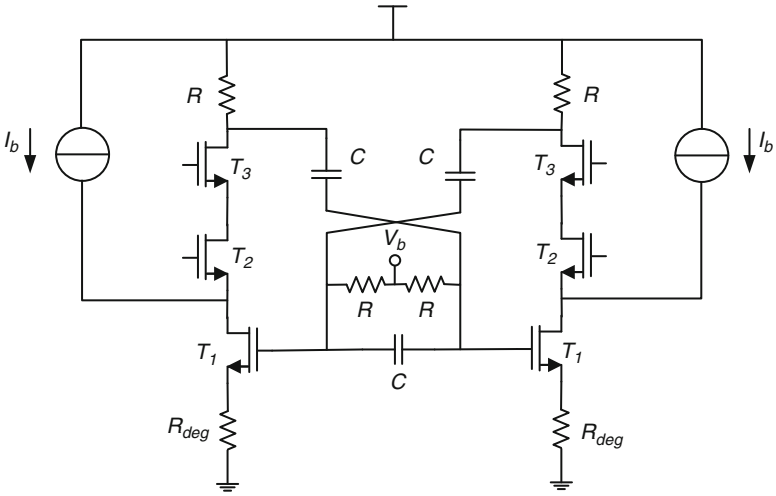

Fig. 2.6 More detailed circuit diagram of a Wien-bridge RC oscillator

output impedance, current bleeding has been applied. The gain-boosted cascode transistors further increase the output impedance such that it does not interfere with the Wien-bridge network's transfer function. To minimize excess phase shift, the cascode transistors are minimum size devices.

The harmonic Wien-bridge RC oscillator of [40] was implemented in a 65 nm CMOS process and dissipates 55 μA from a 1.2 V supply. With $R = 50\text{k}\Omega$, and $C = 530\text{fF}$, it oscillates at about 6 MHz. Its measured absolute accuracy (for six devices characterized from 0°C to 120°C) is reported to be 0.9%, with a temperature coefficient of about 86 ppm/°C.

Another Wien-bridge oscillator based on [40] was proposed in [43], where the RC oscillator circuit is combined with a low drop out voltage regulator in order to achieve a supply dependency of 104 ppm/V. The proposed circuit oscillates at 24 MHz and was implemented in 0.13 μm CMOS. It operates from a supply voltage range of 0.4–1.4 V and dissipates 37 μA. No measurement results were reported on its performance over temperature.

2.5 RC Relaxation Oscillators

Another type of RC-based oscillator is the relaxation oscillator. This produces a digital (square-wave) output signal [47]. Its output frequency can range from hundreds of kHz to a few tens of MHz. In this case, the period of oscillation is proportional to a time constant, determined by a reference voltage, a bias current I_{ref} and a capacitor C (see Fig. 2.7). Since the bias current typically involves a

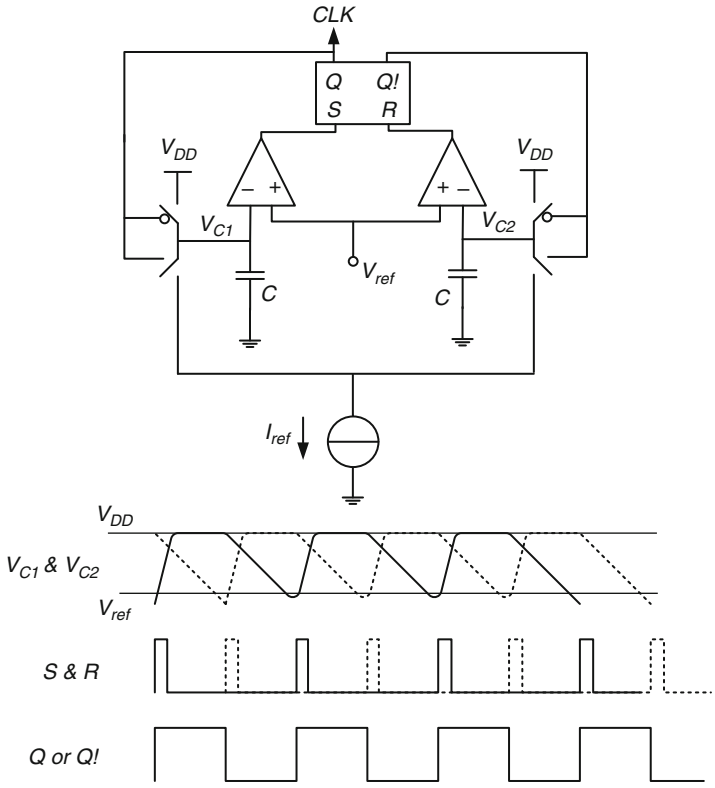

Fig. 2.7 A relaxation oscillator and its waveforms

resistance (e.g. by forcing a band-gap reference voltage across a resistor), they are also recognized as RC oscillators.

CMOS compatibility and very low power operation are some of the major advantages of relaxation oscillators. These characteristics make them suitable for battery powered applications such as the wake-up timers in implantable biomedical systems [48–50]. However, one of their main drawbacks is the dependence of their output frequency on process and temperature variations [48, 49]. This is mainly limited to about 20% by the tolerance and temperature dependence of conventional on-chip resistors and capacitors. By means of temperature compensation and trimming, stabilities of 2% have been achieved [49, 50], sufficient for the previously mentioned applications.

One possible realizations of a relaxation oscillator is shown in Fig. 2.7. This circuit includes a current and a voltage reference, two capacitors and comparators as well as a set-reset (SR) latch. Its operation involves charging capacitors C_1 and C_2 to V_{DD} and then discharging them to V_{ref} by means of I_{ref} (see the waveforms in Fig. 2.7). The Schmitt trigger comparators compare the capacitor voltages with V_{ref}

and change the state of the SR latch, which, in turn, changes the charge and discharge order of the capacitors [50]. The oscillation frequency is determined by:

$$1/f_{osc} = T_{osc} = \frac{C}{2 \cdot I_{ref}} \left[2 \cdot \left(V_{DD} - V_{ref}\right)\right]. \tag{2.4}$$

The flicker ($1/f$) noise of the current reference I_{ref}, as well as the input referred noise of the comparators both contribute to the output jitter. Furthermore, the input referred offset and the process and temperature dependent delay of the comparators will influence the oscillator's accuracy. Various solutions to these issues have been addressed in [50–53].

The designs described in [48, 49] are based on the circuit shown in Fig. 2.7. The reference current and voltage are based on a band-gap reference generator and an 8-bit digital trim can be applied to the oscillator. Without trimming, the reported accuracy of the 12 MHz output frequency is about ±25%, which after trimming (single point) remains stable to ±5% over supply variations and a temperature range of −40°C to 125°C. A 0.5 µm CMOS realization reported in [48] dissipates about 3 µW and its output jitter is in the order of 0.1%. The realization in [49] improves on [48] by reducing the inaccuracy to ±2.5% under the same conditions, which is achieved by correcting for the residual temperature coefficient of the oscillator after the trimming.

The relaxation oscillator presented in [50] is intended for low power biomedical applications. The oscillator is implemented in a 0.13 µm CMOS process, and produces an output frequency of 3.2 MHz. It dissipates 38.4 µW from a 1.5 V supply. The oscillator is also based on the topology shown in Fig. 2.7, with the application of an auto-zeroing mechanism [51] to the oscillator's comparators. This reduces their offset and flicker noise, which improves the oscillator's accuracy and reduces its output jitter, respectively. An 8-bit digital trim of the reference current of the oscillator has a resolution of 0.3%. The reported variation in the output frequency over a temperature range of 20–60°C is ±0.25%. The oscillator's cycle-to-cycle jitter is 524 ps (rms) without the application of auto-zeroing, which drops to 455 ps (rms) when the comparators are auto-zeroed.

A voltage-controlled-oscillator (VCO) based on a relaxation oscillator is presented in [52], with the aim of achieving improved control linearity and jitter performance. An alternative Schmitt trigger circuit is introduced as the oscillator's comparator. The oscillator dissipates 360 µA and has a jitter of 65 ppm (rms) at an oscillation frequency of 1.5 MHz. Its control linearity is affected by the comparator delay, which needs to be minimized compared to the period of oscillation. This could be solved by increasing the comparator bandwidth at the cost of increased noise and jitter [52]. However, in [52] the direction of the capacitor's charging current is changed gradually rather than instantaneously. The accuracy of this oscillator is not reported in [52].

The 12.5 MHz relaxation oscillator described in [53] is implemented in a 65 nm CMOS process and has a current consumption of 70 µA with a 1.2 V supply. This work focuses on the reduction of comparator noise to reduce the total oscillator's

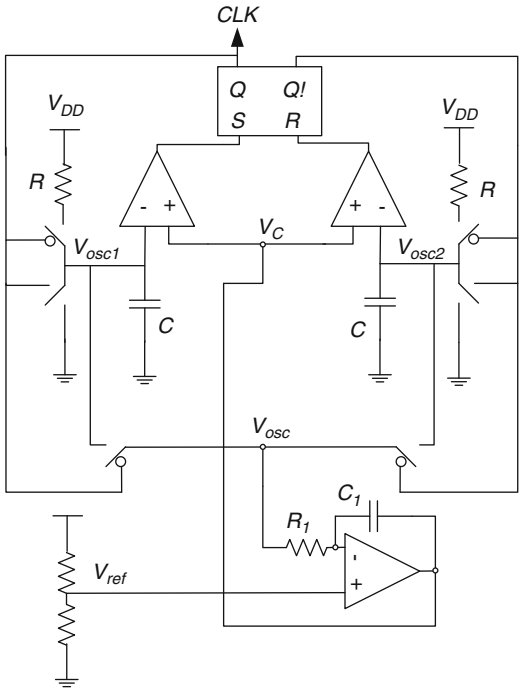

Fig. 2.8 A relaxation oscillator with voltage-averaging feedback

phase noise and jitter. Subtraction of charge by a switched capacitor circuitry filters the comparator noise, which then allows its power consumption to be significantly reduced. The measured phase noise of this oscillator is −82dBm at an offset frequency of 100 kHz. There is no characterization of the temperature stability of this oscillator reported in the corresponding publication.

As described earlier, one of the variables contributing to the output frequency variation of a relaxation oscillator is the delay of its comparator. This is the time it takes the comparator to change the state of the latch after the capacitor voltage reaches V_{ref} (see Fig. 2.7). This delay forms part of the oscillation period, and increases its spread as a function of PVT. This delay can be minimized in comparison to the oscillation period, but at the cost of excess power consumption. The work in [54] proposes a voltage-averaging feedback loop that makes the oscillation period insensitive to the comparator delay.

The voltage-averaging feedback topology [54] is shown in Fig. 2.8. The core of the oscillator can be seen as a relaxation oscillator with two comparators and a control voltage V_C, which is tuned by the voltage averaging feedback circuitry. The two internal voltages V_{osc1} and V_{osc2} (see Fig. 2.9) are alternately applied to the active filter in the voltage averaging feedback circuitry. The active filter made of resistor R_1, capacitor C_1 and an opamp ensures that at all conditions the DC value of V_{osc} is equal to V_{ref}. This means that these two voltages are virtually shorted in a low-frequency bandwidth determined by $R_1 \cdot C_1$ (about 160 kHz with $R_1 = 1\text{M}\Omega$ and $C_1 = 1$ pF). Assuming an ideal opamp in the feedback circuit and

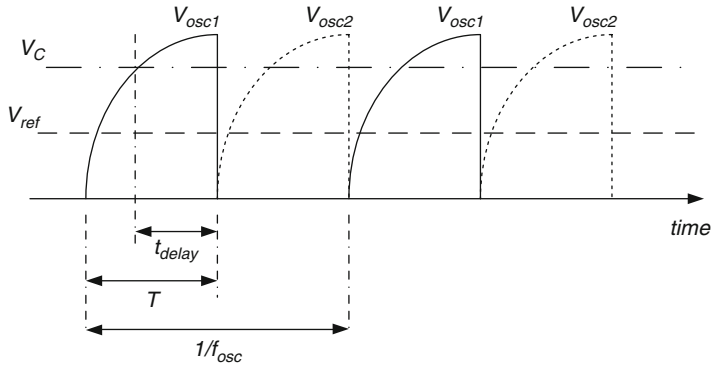

Fig. 2.9 Waveforms of the voltage-averaging relaxation oscillator

considering that the main oscillator capacitor C is being charged to V_{dd} through a resistor R ($R_1 >> R$) the waveforms shown in Fig. 2.9 can be modeled as:

$$V_{osc1,2}(t) = V_{dd}\left(1 - e^{-1/RCt}\right). \tag{2.5}$$

Due to the voltage averaging feedback, the DC value of $V_{osc1,2}$ needs to be equal to V_{ref} in half of an oscillation period (T):

$$\frac{1}{T}\int_0^T V_{osc1,2}(t)dt = V_{ref}. \tag{2.6}$$

As shown by Fig. 2.8, the reference voltage V_{ref} is made by a resistive divider from V_{dd} with a division factor $\alpha = V_{ref}/V_{dd}$. Therefore, (2.6) results in [54]:

$$\frac{(1-\alpha)T}{RC} = 1 - e^{-T/RC}. \tag{2.7}$$

Which means that the oscillation period is ideally only defined by R, C and α. Therefore, variations in comparator delay will have no effect on the oscillation period, because the voltage averaging feedback loop controls V_C to keep the frequency constant. Furthermore, (2.7) shows that the dependence of oscillation period on supply voltage is cancelled. Finally, the low-pass nature of the voltage averaging network (active integrator in the feedback) means that the low frequency (flicker) noise referred to the input of the oscillator will be high-pass filtered, which results in a reduction of the output jitter [54]. The 0.18 μm standard CMOS oscillator presented in [54] dissipates 25 μA from a 1.8 V supply. The reported accuracy of the oscillator's 14 MHz output frequency is ±0.19% (result of a single device) from −40°C to 125°C, while its cycle-to-cycle jitter is 30 ps (rms).

2.6 Ring Oscillators

Ring oscillators are widely used as voltage-controlled oscillators in jitter sensitive applications such as phase-locked loops and clock recovery circuits. This is due to the high frequencies that they can achieve and their relatively simple integration [55]. Ring oscillators are widely realized in CMOS process as a ring of cascaded inverter stages [56]. The number of inverters needs to be odd and the output of the last stage has to be fed back to the input of the first stage (see Fig. 2.10). For an odd number of stages, the output of the last stage is the inverse of the input of the first stage. Propagation delay of the cascaded stages delays the output of the last stage compared to the input of the first stage. This results in the oscillation to propagate in the ring. A half period of oscillation will be equal to the number of inverter stages times the delay of each stage.

The inverter stages could also be made by means of analog delay stages such as the ones published in [57, 58] and shown in Fig. 2.11. This fully differential delay stage is made of a differential pair and a symmetrical load. The time delay introduced by this stage is approximated by [59]:

$$t_d \approx \frac{C_0(V_H - V_L)}{I_{ref}}. \tag{2.8}$$

Where C_0 is the total capacitance at the output of the stage, I_{ref} is the bias current of the circuit and $V_H - V_L$ is the output voltage swing, determined by V_{ref} and V_{CTRL}

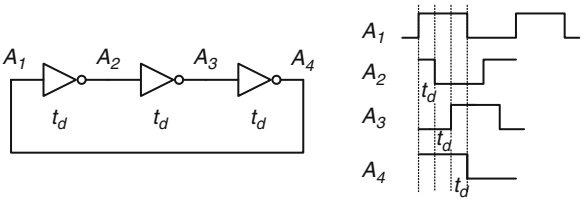

Fig. 2.10 Simplified ring oscillator schematic and its conceptual timing diagram

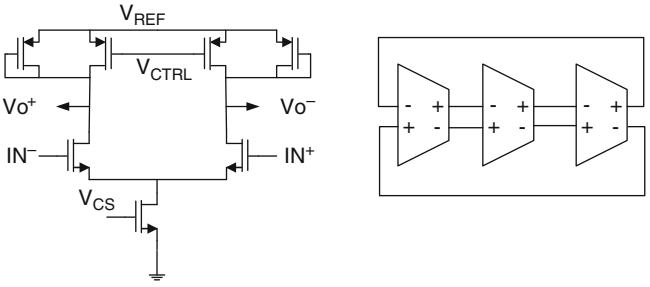

Fig. 2.11 Differential delay cell and a three stage oscillator

[57]. The ring oscillator proposed in [57] is made of a cascade of three delay stages (see Fig. 2.11). To vary the time delay t_d, and thus the output frequency, the control voltage V_{CTRL} can be modified.

The delays of the stages of a ring oscillator vary as a function of PVT. Supply voltage variations affect the voltage domain parameters in (2.8), while the temperature dependence of MOS transistors and passive components affects the reference currents and voltages. In order to reduce these effects, two main approaches can be found in literature. The first approach takes free running and open-loop ring oscillators and compensates the PVT effects within the circuit. The second approach embeds a voltage/current controlled ring oscillator in a feedback loop. As a result of feedback, the output frequency of the ring oscillator is locked to the time constant produced by a temperature compensated resistor and capacitor network. These two approaches will be discussed in the following sub-sections.

2.6.1 Open-Loop Compensation

The work presented in [57] describes how PVT compensation techniques can be applied to a free running, open-loop ring oscillator. An earlier oscillator, presented in [58], had a nominal frequency of 680 kHz and was implemented in a 0.6 μm CMOS process with inaccuracy of ±6.8% from 35°C to 115°C. Later, an improved implementation in a 0.25 μm CMOS process was presented in [57] with an output frequency of 7 MHz. The improved oscillator had an untrimmed inaccuracy of ±2.6% over process, supply and a temperature range of −40°C to 125°C. The reported accuracy is based on the data collected from 94 samples from two different batches. A block diagram of the complete system, including the process and temperature compensation as well as the supply regulation around the core oscillator, is shown in Fig. 2.12.

A band-gap voltage reference regulates the variable supply (2.4–3 V) to a supply and temperature stable 2.2 V reference voltage V_{ref}. This voltage is then used by other blocks in the system. The reference frequency is produced by the differential three stage ring oscillator at the core of the system, whose frequency is stabilized by a reference current I_{ref} (see Fig. 2.11). This current is derived from the control voltage V_{CTRL}, which is generated by the temperature and process compensation circuitry. The analog output of the ring oscillator is translated by a rail-to-rail swing comparator to digital voltage levels.

The control voltage V_{CTRL} is varied to correct for temperature and process variations. The critical temperature dependent parameters are the mobility, $\mu_{P,N}$, and the threshold voltage, $V_{THP,N}$, of the MOS transistors [60]. The mobility has an approximate $T^{-1.5} \sim T^{-2.2}$ temperature dependence, where T is the absolute temperature. The threshold voltage however has a negative temperature coefficient. Furthermore, the junction capacitances of a MOS device as well as the oxide capacitance have temperature dependences [57, 60]. Process variations affect gate oxide thickness and doping concentrations, leading to threshold voltage and

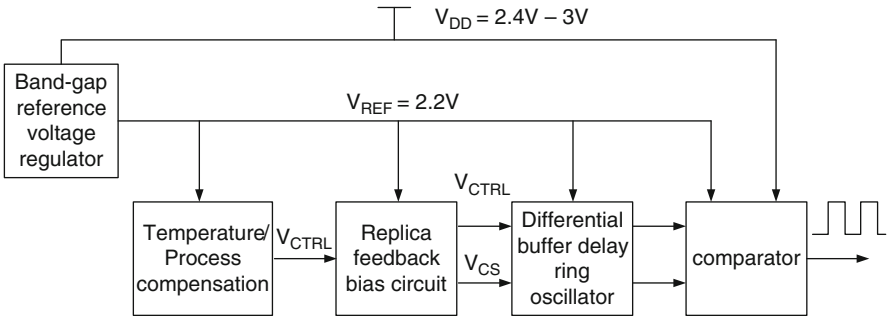

Fig. 2.12 System block diagram of the temperature and process compensated ring oscillator

mobility variations. In [57] a bipolar transistor's base–emitter voltage V_{BE}, which has a negative temperature coefficient [61], was used to correct for the overall negative temperature coefficient of the ring oscillator. Furthermore, a threshold voltage detection circuit detects the process corner and modifies the reference voltage of the oscillator accordingly.

2.6.2 Closed-Loop Compensation

A ring oscillator with temperature compensation feedback loop is described in [62]. The oscillator has an output frequency of 10 MHz, dissipates 80 μW, and has a temperature dependence of 67 ppm/°C. This supply regulated oscillator, has been implemented in a 0.18 μm CMOS process. Its frequency stability is ±0.4% from −20°C to 120°C (data reported for a single device). There is no data available on the jitter performance of this oscillator.

A block diagram of the closed loop oscillator of [62] is shown in Fig. 2.13. The core ring oscillator has four differential stages and its supply, V_{CTRL}, is regulated by a feedback loop. This locks the output frequency of the ring oscillator to a PVT insensitive voltage V_{ref}. To close the feedback loop, a frequency-to-voltage converter (shown in Fig. 2.13) is used, which also realizes a linear temperature compensation scheme. To further investigate the operation of the loop, the timing diagram shown in Fig. 2.14 needs to be considered together with the block diagram of Fig. 2.13.

A voltage regulator based on a band gap reference produces a 1 V voltage V_{REG} from the variable V_{DD} (1.2 ~ 3 V). When the reset signal RST is high, the charge on capacitor C_0 is set such that $V_{cap} = V_{REG}$. After the reset phase, the frequency conversion phase begins with signal Q = 0, discharging C_0 by current I_{ref}. The signal Q is then produced through a frequency divider by dividing the oscillator output frequency by two (see Fig. 2.13). The discharge of C_0 continues until signal Q changes state again. This always happens at the end of the oscillation period. At the rising edge of Q, and for any given value of I_{ref} and C_0, the voltage across

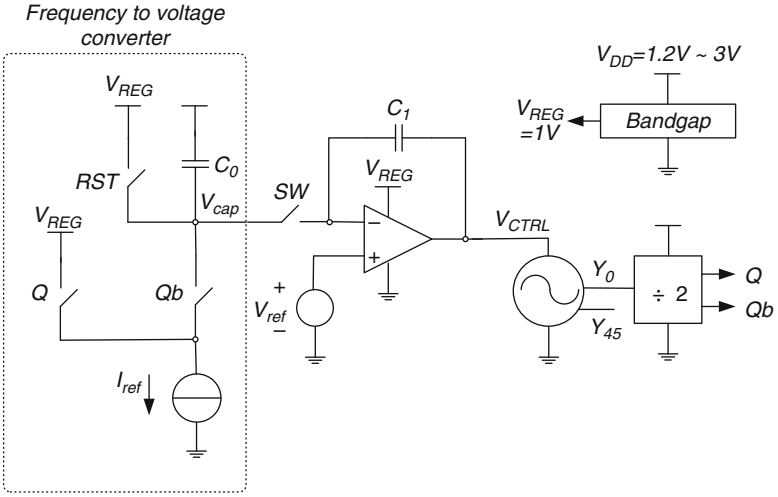

Fig. 2.13 Ring oscillator with a frequency-to-voltage converter and feedback loop

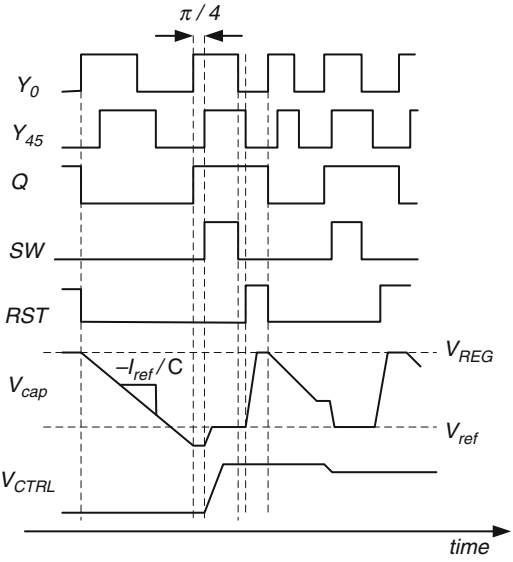

Fig. 2.14 Timing diagram of the ring oscillator in a feedback loop

C_0, V_{cap}, will be a function of the oscillation period. During the time SW = 1 (both SW and RST are generated by a digital control block that is not shown in the figure), V_{cap} is compared to a reference voltage V_{ref} through a switched capacitor loop filter. This works based on charge transfer from C_0 to C_1, which leads to a change in V_{CTRL}. Due to feedback around the integrator, the voltage V_{cap} will be forced to be

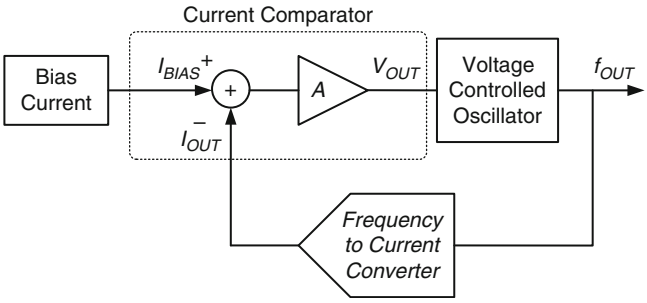

Fig. 2.15 Block diagram of the ring oscillator with frequency to current converter

equal to V_{ref}. Since V_{cap} is a representative of the oscillation period, for a constant V_{ref}, having $V_{cap} = V_{ref}$, is equivalent to having a constant output frequency. At steady-state, the output frequency, f_{CLK}, can be derived from [62]:

$$f_{CLK} = \frac{I_{ref}}{2C_0(V_{REG} - V_{ref})}. \tag{2.9}$$

To ensure a stable output frequency, the values of V_{REG}, V_{ref}, and I_{ref} need to be insensitive to PVT. The first two are made by means of a band-gap voltage reference and a sub-threshold voltage divider, respectively [62].

Another ring oscillator embedded in a control feedback loop is presented in [63]. This is an implementation in a 0.35 μm CMOS with a tunable output frequency from 2 to 100 MHz. The oscillator dissipates 180 μW at 30 MHz and has a process sensitivity of 2.7% and a temperature coefficient of 90 ppm/°C. A simplified block diagram of this oscillator is shown in Fig. 2.15. The circuit includes a bias current generator circuit, a current comparator, a ring oscillator based VCO and a frequency-to-current converter arranged in a frequency-locked loop. The current comparator block produces the output voltage V_{OUT} driving the VCO based on the difference between I_{BIAS} and I_{OUT}. Feedback forces these two currents to be equal.

The complete circuit diagram of the oscillator is shown in Fig. 2.16. It consists of a bias current generator that produces a bias current I_{BIAS} from the series combination of positive and negative temperature coefficient resistors. This is done by copying the bias voltage V_{BIAS} through a feedback amplifier to the resistors. Furthermore, the circuit includes a current comparator made of a simple common-source stage comparing I_{BIAS} and I_{OUT} (the output current of the frequency-to-current converter). The output of this stage is the control voltage V_{OUT}. The core ring oscillator is made of seven current-starved inverter stages. Its oscillation frequency, f_{OUT}, is determined by the applied current I_b to the inverters [63]:

$$f_{OUT} \propto \frac{I_b}{2mC_L V_{DD}}. \tag{2.10}$$

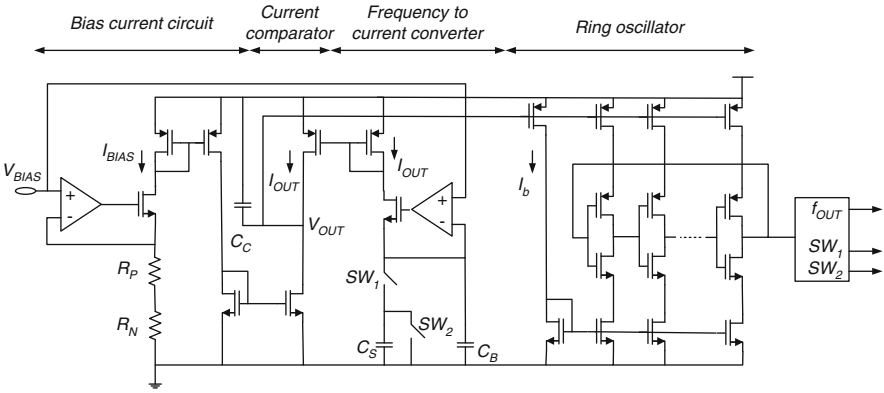

Fig. 2.16 Circuit diagram of ring oscillator with frequency-to-current converter in a feedback loop

Where m is the number of inverters and C_L is each inverter's load capacitance. The variations in control voltage V_{OUT} determine the current I_b and thus the oscillation frequency.

The frequency to current converter is made of a switched capacitor resistance made of capacitor C_S ad two switches $\mathrm{sw}_{1,2}$ that are driven by the output of the oscillator. This means that the switched capacitor resistance is proportional to the oscillation frequency, and therefore, by copying the V_{BIAS} voltage onto this resistor, a frequency dependent output current I_{OUT} will be produced [63]:

$$I_{OUT} = f_{OUT} \cdot C_S \cdot V_{BIAS}. \tag{2.11}$$

A current mirror copies this current to the current comparator. At the steady state of the frequency-locked loop, the oscillation frequency will be given by:

$$f_{OUT} = \frac{1}{(R_P + R_N) \cdot C_S}. \tag{2.12}$$

Where R_P and R_N are the positive and negative temperature coefficient resistors used to produce the I_{BIAS} current from V_{BIAS}. To first order, the residual temperature coefficient of the composite resistor as well as that of the capacitor C_S determines the temperature coefficient of the oscillator.

For the closed-loop ring oscillators discussed so far, the oscillator's frequency is locked to a time constant defined by an RC circuit. These circuits provide a continuous correction of the frequency in response to supply voltage and temperature variations. Their achieved level of PVT variation is determined by that of the RC circuit.

2.7 Mobility-Based Frequency References

Recently, a class of low-power temperature-compensated frequency references based on the mobility of MOS transistors has been introduced [64–66]. Such references dissipate micro watts of power and achieve inaccuracies in the order of a few percent. The implementation described in [65] has been targeted for wireless sensor networks. It has an output frequency of 150 kHz, dissipates 42.6 µA from a 1.2 V supply, and is fabricated in a 65 nm standard CMOS process. For a temperature range of −55°C to 125°C, the reference achieves an output frequency stability of ±0.5% when trimmed at two temperature points. With a single trim its inaccuracy is ±2.7%. Another mobility based oscillator reported in [66] has been implemented in a 0.35 µm CMOS, has an output frequency of 3.3 kHz, and consumes 11nW from a 1 V supply.

The temperature dependence of mobility is in the order of $T^{-1.6}$ [65], which means that temperature compensation needs to be applied to a mobility based frequency reference. The core of the reference proposed in [65] is a current-controlled relaxation oscillator, which is controlled by a current that is proportional to the electron mobility. The temperature compensation of the oscillator is performed digitally (see Fig. 2.17). A band-gap temperature sensor [67] measures the temperature of the die. Through a non-linear digital mapping, the sensor's digital output is translated into a temperature-dependent division factor N_{div}, which is then applied to a divider. This divides the oscillator's output frequency by N_{div} in order to produce a stable output frequency f_{osc}.

A simplified circuit schematic of the mobility-based oscillator as well as its timing diagram is shown in Fig. 2.18. The voltage difference between the gates of M_1 and M_3 is kept equal to V_R by the combination of the current source I_0, R_0 and OA_1 [65]. Using the square-law MOS model, the drain current of M_1 is determined by:

$$I_1 = \frac{\mu_n C_{ox}}{2} \frac{W_1}{L_1} \frac{V_R^2}{\left(\sqrt{\frac{n}{m}} - 1\right)^2}. \tag{2.13}$$

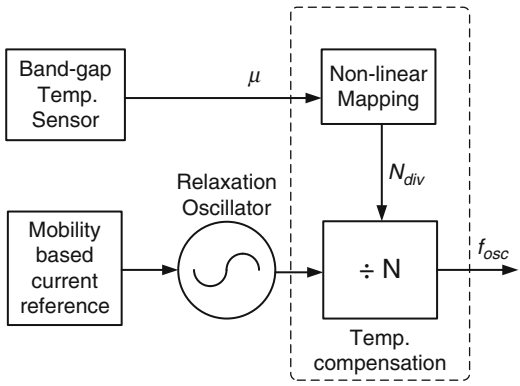

Fig. 2.17 Simplified block diagram of the temperature compensated mobility based frequency reference

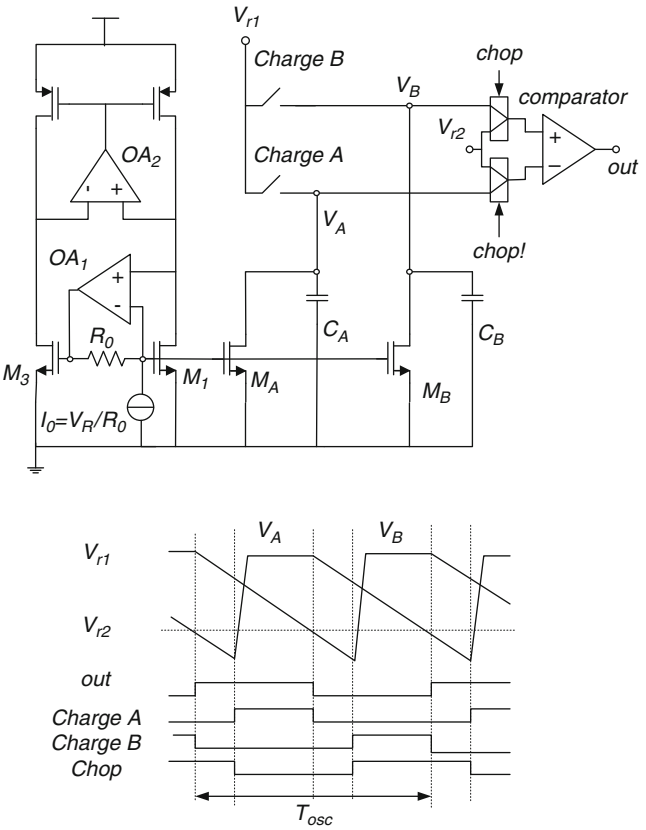

Fig. 2.18 Circuit and timing diagrams of the mobility based frequency reference

where m = $(W/L)_3/(W/L)_1$ and n = $(W/L)_4/(W/L)_2$, μ_n is the electron mobility, C_{ox} is the oxide capacitance of the MOS transistor per unit area. The current source I_0 is implemented by mirroring the current flowing in a resistor matched to R_0 whose voltage drop is equal to the reference voltage V_R (not shown in the schematic).

The drain current of M_1 is mirrored by M_A and M_B with a gain of four and used to alternatively discharge C_A and C_B after they have been pre-charged to V_{r1}.A comparator changes the state of charge and discharge of capacitors when the voltage on the discharging capacitor drops below V_{r2}. The oscillation frequency of this oscillator can be derived from [65]:

$$f_{osc} = \frac{\mu_n C_{ox}}{4C\left(\sqrt{\frac{n}{m}} - 1\right)^2} \cdot \frac{W_1}{L_1} \cdot \frac{V_R^2}{V_{r1} - V_{r2}}. \tag{2.14}$$

where $C = C_A = C_B \propto C_{ox}$.

A band-gap temperature sensor based on a bipolar core including NPN transistors and a first order delta-sigma ADC produces a digital representation of the die temperature [67]. The temperature sensor's accuracy should not limit the compensated oscillator's output frequency stability. For a frequency error of about 0.3%, the temperature sensor's accuracy needs to be better than 0.5°C [65]. A division factor N_{div} with 13-bits resolution has been chosen. A seventh order polynomial with fixed coefficients is used to translate the output of the temperature sensor to the division factor N_{div}.

Another relaxation oscillator locked to the mobility of MOS transistors has been implemented in a 0.35 μm CMOS process and is reported in [66]. This oscillator has an output frequency of 3.3 kHz and consumes 11nW from a 1 V supply. Its reported temperature drift from −20°C to 80°C is 500 ppm/°C, which accounts for a total temperature variation of about 5%. The key features in this topology are the generation of an electron mobility based reference current and the production of an oscillator reference voltage with the same temperature dependence as the electron mobility, to temperature compensate the output frequency. Further power reduction has been achieved by using a relaxation oscillator based on a single comparator and reducing the power consumption of the digital circuitry by means of a reduced supply voltage operation through a voltage regulator. The reported process spread of this oscillator, measured at a single temperature point, amounts to about ±15% [66].

2.8 Comparison

This chapter provided an overview of the various types of silicon-based frequency references. These included MEMS-resonator-based oscillators, LC oscillators, RC harmonic oscillators, RC relaxation oscillators, ring oscillators and finally electron-mobility-based oscillators. Each approach has its own specific advantages and disadvantages. To make a comparison, it is helpful to summarize the performance characteristics for each type of frequency reference.

One of the difficulties in providing a complete and fair comparison between published frequency references is that often insufficient data on their performance over process and temperature has been provided. There are references in which the performance of a single device has been reported as a measure of stability, which does not allow a fair comparison with references for which more samples have been characterized. From the previously described types of silicon-based frequency references, a performance summary of those with the most complete results is presented in Table 2.1.

MEMS-resonator-based oscillators and LC oscillators have been commercialized, and thus their reported performance characteristics are at production level. The characteristics of other topologies are obtained mainly from publications. It can be seen that MEMS-based oscillators achieve the best accuracy over the widest temperature range. Their form factor has also been shrunk and they

Table 2.1 Comparison of some state-of-the-art all-silicon frequency references

Reference number	[23]	[32]	[43]	[57]	[65]	[54]
Reference's principle of operation	MEMS	LC	RC harmonic	Ring	Mobility	Relaxation feedback
Frequency range	1–800 MHz	24 MHz	6 MHz	7.03 MHz	150 kHz	14 MHz
Temperature range (°C)	−40 to 125	0–70	0–120	−40 to 125	−55 to 125	−40 to 125
Supply voltage (V)	1.8–3.3	1.8	1.2	2.5	1.2	1.8
Power consumption (or supply current)	3.2–20 mA	<4 mW	66 µW	1.5 mW	51 µW	45 µW
Area (mm^2)	Not available	0.8	0.03	1.6	0.2	0.04
Process	MEMS + CMOS	0.13 µm	65 nm	0.25 µm	65 nm	0.18 µm
Accuracy (ppm)	20–100	±300	±9,000	±18,400	±5,000 (two point rrim) and ±27,000 (single trim)	±1,900
Temperature coefficient (ppm/°C)	Not available	±8.6	±86	±50.9	Not available	±23
Period jitter (rms)	<5 ps	<2 ps	Not available	Not available	52 ns	30 ps
Number of samples reported	Commercial	Commercial	6	94	12	1

are physically smaller than crystal oscillators. However, their major disadvantage is their need for special MEMS processing. This requires a two-die solution, in which the MEMS resonator is wire bonded to another CMOS chip. The power consumption of MEMS oscillators is comparable to LC oscillators and is larger than the other types.

Apart from the MEMS-based oscillators, all the other frequency references in Table 2.1 are standard CMOS compatible, which is a great advantage as far as manufacturing and packaging costs and complexity are considered. Among these, LC oscillators achieve the best accuracy over process and temperature, as well as the best jitter performance. However, their power consumption is higher than the rest and their temperature range is the narrowest. MEMS-based and LC-based oscillators are the only solutions that can achieve accuracies better than 0.1% at a reasonable jitter level.

For less accurate applications with stability requirements above 1% and with stringent power consumption requirements, RC, mobility-based, and relaxation oscillators can be used. These oscillators have very low chip area and can operate at the micro-Watt range. They are well suited for battery powered applications such as wireless sensor networks or biomedical implants.

2.9 Conclusions

Most electronic devices require a frequency reference. The stability of this reference, i.e. its deviation as a function of PVT, is crucial for many applications. For decades, crystal oscillators have been the dominant frequency control components. So far, they have achieved the best stability and noise/jitter performance; however, they have a few drawbacks. Their integration in the IC technology is nearly impossible. Furthermore, they are sensitive to shock and vibration, which can cause reliability problems.

In order to replace the crystal oscillators, there has been a tremendous R&D effort over the past few years. The goal is to produce integrated frequency references that can achieve the stability of crystal oscillators. This is justified by the large market for frequency generation and control components. Furthermore, an integrated, or in other words all-silicon, frequency reference brings added-value in terms of reliability and reduced area and cost.

One of the successfully commercialized all-silicon frequency references is the MEMS resonator based oscillator. This requires a two-die solution that combines a MEMS resonator with a CMOS chip. MEMS oscillators already achieve levels of stability below 1 ppm, which is comparable to that of crystal oscillators. Their stability is not altered by shock and vibration and their form factor allows for their placement in the same foot print as the crystal oscillators.

It will be still more advantageous if an all-silicon frequency reference could be made that is standard CMOS compatible. This would allow for cheap and simple production and packaging, as well as integration in systems-on-chip. So far, such

references have been based on time constants produced by means of on-chip passive elements such as resistors, capacitors and inductors.

Among such CMOS compatible oscillators, the LC type has so far become commercial with stabilities in the order of a few tens of ppm's. This is achieved by means of trimming and temperature compensation. The RC type oscillators have stabilities in the order of 1%; however, their power consumption is much lower than that of LC oscillators, allowing for their use in battery powered applications. Furthermore, temperature compensated oscillators locked to the electron mobility of MOS transistors have been recently introduced achieving stabilities in the order of 1%.

The all-silicon oscillators reviewed so far in this chapter are based on signals which are produced, transferred and processed in the mechanical, electrical and magnetic energy domains. This is mainly done through the use of electromechanical structures or electrical passive components in combination with electronic circuitry. The main focus of this book is on investigating the possibility of accurate on-chip frequency generation through the generation and transfer of signals in another physical energy domain: the thermal domain. The ultimate goal is to make an accurate CMOS-compatible frequency reference. In the following chapters, the design of an electrothermal frequency reference based on the thermal properties of IC grade silicon will be investigated.

References

1. Bottom VE (1981) A history of the quartz crystal industry in the USA. In: IEEE annual frequency control symposium, Philadelphia, Pennsylvania, pp 3–12
2. Allan D et al (1997) The science of timekeeping, HP Application Note 1289
3. Lam CS (2008) A review of the recent development of MEMS and crystal oscillators and their impacts on the frequency control products industry. In: IEEE ultrasonic symposium, pp 694–704
4. McCorquaodale MS et al (2009) On modern and historical short-term frequency stability metrics for frequency sources. In: IEEE frequency control symposium, pp 328–333
5. Oscillators for microcontrollers, Intel Application Note AP-155, 1983
6. Universal Serial Bus (USB) Specifications Rev 3.0, 2008. Available online at: www.usb.org
7. Allan DW et al (1988) Ensemble time and frequency stability of GPS satellite clocks. In: IEEE annual frequency control symposium, pp 465–471
8. McCorquodale MS (2009) Silicon challenges quartz: precision self-referenced solid-state oscillators for frequency control and generation. In: IEEE Toronto section, University of Toronto, Canada, 2009. Available online at: www.toronto.ieee.ca/chapters/ssc/mccorquodaleUToronto09.pdf
9. Nathanson HC et al (1967) The resonant gate transistor. IEEE Trans Electron Dev 14 (3):117–133
10. Sadiku M (2002) MEMS. IEEE Potential 21(1):4–5
11. Nathanson HC et al (1965) A resonant-gate silicon surface transistor with high-Q bandpass properties. IEEE Trans Electron Dev 12(9):507
12. Tabatabaei S et al (2010) Silicon MEMS oscillators for high-speed digital systems. IEEE Micro 30(2):80–89
13. MEMS replacing quartz oscillators, SiTime Application Note AN10010, 2009

14. Lutz M (2007) MEMS oscillators for high volume commercial applications. In: IEEE transducers, pp 49–52
15. Wan-Thai Hsu et al (2007) The new heart beat of electronics - Silicon MEMS oscillators. In: IEEE electronic components and technology conference, ECTC, pp 1895–1899
16. Ruffieux D et al (2010) Silicon resonator based 3.2 uW real time clock with 10 ppm frequency accuracy. IEEE J Solid-State Circ 45(1):224–234
17. Perrott MH et al (2010) A low-area switched-resistor loop-filter technique for fractional-N synthesizers applied to a MEMS based programmable oscillator. In: IEEE international solid-state circuits conference, ISSCC, pp 244–245
18. Nguyen CT-C (2007) MEMS technology for timing and frequency control. In: IEEE transactions on ultrasonics, ferroelectrics and frequency control, pp 251–270
19. Galton I (2002) Delta-sigma data conversion in wireless transceivers. IEEE Trans Microw Theory Tech 50:302–315
20. Wan-Thai Hsu (2006) Reliability of silicon resonator oscillators. In: IEEE international frequency control symposium and exposition, pp 389–392
21. SiT8003XT, SiT8102, and SiT9102 data sheets from SiTime. Available online at: www.sitime.com
22. DSC1018 data sheet from Discera. Available online at: www.discera.com
23. SiTime's product selector sheet. Available online at: http://www.sitime.com/support/product-selector
24. IDT data sheets of MM8102, MM8103, and MM8103. Available online from www.idt.com
25. Hajimiri A (1999) Design issues in CMOS differential LC oscillators. IEEE J Solid-State Circ 34(5):717–724
26. Zannoth M et al (1998) A fully integrated VCO at 2 GHz. IEEE J Solid-State Circ 33(12):1987–1991
27. McCorquodale MS et al (2007) A monolithic and self-referenced RF LC clock generator compliant with USB 2.0. IEEE J Solid-State Circ 42(2):385–399
28. McCorquodale MS et al (2008) A 0.5-to-480 MHz self-referenced CMOS clock generator with 90 ppm total frequency error and spread-spectrum capability. In: IEEE international solid-state circuits conference, ISSCC, pp 350–351
29. McCorquodale MS et al (2008) A 25 MHz All-CMOS reference clock generator for XO-replacement in serial wire interfaces. In: IEEE international symposium on circuits and systems, ISCAS, pp 2837–2840
30. McCorquodale MS et al (2008) Self-referenced, trimmed and compensated RF CMOS harmonic oscillators as monolithic frequency generators. In: IEEE frequency control symposium, pp 408–413
31. McCorquodale MS et al (2009) A 25-MHz self-referenced solid-state frequency source suitable for XO-replacement. IEEE Trans Circ Syst I Regular Pap 56(5):943–956
32. McCorquodale MS et al (2010) A silicon die as a frequency source. In: IEEE international frequency control symposium, pp 103–108
33. Groves R (1997) Temperature dependence of Q and inductance in spiral inductors fabricated in a silicon-germanium/BiCMOS technology. IEEE J Solid-State Circ 32(9):1455–1459
34. McCorquodale MS et al (2011) A history of the development of CMOS oscillators: the dark horse in frequency control. In: IEEE international frequency control symposium, pp 437–442
35. Data sheet of Si500 silicon oscillators. Available from the website of Silicon Labs at: www.silabs.com
36. Wikipedia page on RC oscillators. Available online at: http://en.wikipedia.org/wiki/RC_oscillator
37. McCreary JL (1981) Matching properties, and voltage and temperature dependence of MOS capacitors. IEEE J Solid-State Circ 16(6):608–616
38. St Onge SA et al (1992) Design of precision capacitors for analog applications. IEEE Trans Compon Hybr Manufact Technol 15(6):1064–1071

39. Lane WA et al (1992) The design of thin-film polysilicon resistors for analog IC applications. IEEE Trans Electron Dev 36(4):738–744
40. De Smedt V et al (2009) A 66 μW 86 ppm/°C fully-integrated 6 MHz wienbridge oscillator with a 172 dB phase noise FOM. IEEE J Solid-State Circ 44(7):1990–2001
41. Paavola M et al (2006) A 3 μW, 2 MHz CMOS frequency reference for capacitive sensor applications. In: IEEE international symposium on circuits and systems, ISCAS, pp 4391–4394
42. Blauschild RA (1994) An integrated time reference. In: IEEE international solid-state circuits conference, ISSCC, pp 56–57
43. De Smedt V et al (2009) A 0.4–1.4 V 24 MHz fully integrated 33 μW, 104 ppm/V supply-independent oscillator for RFIDs. In: IEEE European solid-state circuits conference, ESSCIRC, pp 396–399
44. Wikipedia page on wienbridge oscillators. Available online at: http://en.wikipedia.org/wiki/Wien_bridge_oscillator
45. Model 200A Audio Oscillator, 1939, description from HP virtual museum. Available online at: http://www.hp.com/hpinfo/abouthp/histnfacts/museum/earlyinstruments/0002/index.html
46. Hewlett WR (1939) Variable frequency oscillation generator, patent filed on 11 July 1939
47. Johns DA, Martin K (1997) Analog integrated circuits. Wiley, New York
48. Olmos A (2003) A temperature compensated fully trimmable on-chip IC oscillator. In: IEEE symposium on integrated circuits and systems design, pp 181–186
49. Vilas Boas A et al (2004) A temperature compensated digitally trimmable on-chip IC oscillator with low voltage inhibit capability. In: IEEE international symposium on circuits and systems, ISCAS, pp 501–504
50. Choe K et al (2009) A precision relaxation oscillator with a self-clocked offset-cancellation scheme for implantable biomedical SoCs. In: IEEE international solid-state circuits conference, ISSCC, pp 402–403
51. Enz CC et al (1996) Circuit techniques for reducing the effects of op-amp imperfections: autozeroing, correlated double sampling, and chopper stabilization. Proc IEEE 84 (11):1584–1614
52. Gierkink SLJ, van Tuijl E (2002) A coupled sawtooth oscillator combining low jitter with high control linearity. IEEE J Solid-State Circ 37(6):702–710
53. Geraedts et al PFJ (2008) A 90 μW 12 MHz relaxation oscillator with a –162 dB FOM. In: IEEE international solid-state circuits conference, ISSCC, pp 348–349
54. Tokunaga Y et al (2010) An on-chip CMOS relaxation oscillator with voltage averaging feedback. IEEE J Solid-State Circ 45(6):1150–1158
55. McNeill JA (1997) Jitter in ring oscillators. IEEE J Solid-State Circ 32(6):870–879
56. Wikipedia page on ring oscillators. Available online at: http://en.wikipedia.org/wiki/Ring_oscillator
57. Sundaresan K et al (2006) Process and temperature compensation in a 7-MHz CMOS clock oscillator. IEEE J Solid-State Circ 41(2):433–442
58. Shyu Y et al (1999) A process and temperature compensated ring oscillator. In: IEEE Asia Pacific conference on ASICs, pp 283–286
59. Maneatis JG (1996) Low-jitter process-independent DLL and PLL based on self-biased techniques. IEEE J Solid-State Circ 31(11):1723–1732
60. Razavi B (2000) Design of analog CMOS integrated circuits. McGraw-Hill, Boston
61. Pertijs MAP, Huijsing JH (2006) Precision temperature sensors in CMOS technology. Springer, Dordrecht
62. Lee J et al (2009) A 10 MHz 80 μW 67 ppm/°C CMOS reference clock oscillator with a temperature compensated feedback loop in 0.18 μm CMOS. In: IEEE symposium on VLSI circuits, pp 226–227
63. Ueno K et al (2009) A 30-MHz, 90-ppm/°C fully-integrated clock reference generator with frequency-locked loop. In: IEEE European solid-state circuits conference, ESSCIRC, pp 392–395

64. Sebastiano F et al (2009) A low-voltage mobility-based frequency reference for crystal-less ULP radios. IEEE J Solid-State Circ 44(7):2002–2009
65. Sebastiano F et al (2011) A 65-nm CMOS temperature-compensated mobility-based frequency reference for wireless sensor networks. IEEE J Solid-State Circ 46(7):1544–1552
66. Denier U (2010) Analysis and design of an ultralow-power CMOS relaxation oscillator. IEEE Trans Circ Syst-I Regular Pap 57(8):1973–1982
67. Sebastiano F et al (2010) A 1.2-V 10-μW NPN-based temperature sensor in 65-nm CMOS with an inaccuracy of 0.2 °C (3σ) from −70 °C to 125 °C. IEEE J Solid-State Circ 45 (12):2591–2601

http://www.springer.com/978-1-4614-6472-3

Electrothermal Frequency References in Standard CMOS

Kashmiri, S.M.; Makinwa, K.A.A.

2013, IX, 214 p., Hardcover
ISBN: 978-1-4614-6472-3